Pure Appl. Chem., Vol. 83, No. 1, pp. 213–232, 2011.
doi:10.1351/PAC-CON-10-09-16

Fluorescent ribonucleoside analogues as probes for investigating RNA structure and function*

Seergazhi G. Srivatsan‡ and Anupam A. Sawant

Indian Institute of Science Education and Research, Sai Trinity Building, Pashan, Pune 411021, India

Abstract: Numerous biophysical tools based on fluorescence have been developed to advance the understanding of RNA–nucleic acid, RNA–protein, and RNA–small molecule interactions. In this regard, fluorescent ribonucleoside analogues that are sensitive to their local environment provide sensitive probes for investigating RNA structure, dynamics, and recognition. Most of these analogues closely resemble the native ribonucleosides with respect to their overall dimension and have the ability to form canonical Watson–Crick (WC) base pairs. Therefore, it is possible to place these probes near the point of interaction in a target nucleic acid with minimum structural perturbations and gain insight into the intricacies of conformational changes taking place in and around the interaction site. Here, we provide a concise background on the development and recent advances in the applications of base-modified fluorescent ribonucleoside analogue probes. We first present various base-modified fluorescent ribonucleoside analogues, their photophysical properties, and methods to incorporate these analogues into oligoribonucleotides. We then discuss the established spectroscopic techniques, which make use of the fluorescence properties of these emissive ribonucleoside analogues. Finally, we present the applications of base-modified fluorescent ribonucleoside analogues used as probes incorporated into oligoribonucleotides in investigating RNA structures and functions.

Keywords: assay development; fluorescence; fluorescent ribonucleosides; RNA structure; RNA dynamics.

INTRODUCTION

In contemporary biology, RNAs are recognized as functionally sophisticated biopolymers participating in diverse cellular functions. The functional diversity of RNAs originates from their ability to fold into a number of secondary structure elements, which are crucial for a variety of binding events with other biomolecules that are central elements in biological processes [1–3]. The discovery of the gene regulation phenomenon called RNA interference (RNAi) by noncoding RNAs has been considered as one of the seminal contributions of this decade [4,5]. In most eukaryotic cells, RNAi is an evolutionarily conserved pathway for regulating gene expression in which small RNA molecules, microRNA (miRNA) or small interfering RNA (siRNA), bind to a specific mRNA target and either increase or decrease protein expression [6,7]. In view of the fact that RNAi-based gene regulation is highly potent and selective, it

Pure Appl. Chem.* **83, 1–252 (2011). A collection of invited, peer-reviewed articles by former winners of the IUPAC Prize for Young Chemists, in celebration of the International Year of Chemistry 2011.

‡Corresponding author: E-mail: srivatsan@iiserpune.ac.in

has become the method of choice for silencing several disease-associated genes in mammalian cells. Recent studies have demonstrated that RNAi phenomenon can be harnessed to silence oncogens and other genes involved in cell proliferation, differentiation, and apoptosis [8,9].

Another seminal contribution after RNAi is the discovery of metabolite-dependent gene regulation by riboswitches in bacteria, and in certain plants and fungi [10,11]. Riboswitches are noncoding RNA motifs of respective mRNAs that bind to cognate small-molecule metabolites in a concentration-dependent manner. This binding event results in the structural reorganization of the mRNA, which is translated into a signal that modulates the gene that it codes, and hence, the biosynthesis of the metabolite itself. Recent reports on the mechanism of action of certain antibacterial drugs discovered decades ago suggest that these molecules function at least in part by targeting riboswitches [12]. Therefore, riboswitches are currently being seriously considered as potential antibacterial drug targets.

Bacterial ribosome has been one of the oldest and most well studied targets of a class of naturally occurring and structurally related antibiotics, the aminoglycosides [13]. These aminoglycoside antibiotics bind to the bacterial ribosomal decoding site (A-site) of 16S rRNA and induce codon-anticodon misreading resulting in mistranslation as well as translocation inhibition. Aminoglycosides have also been found to inhibit the activity of ribozymes such as self-splicing group I introns and the hammerhead (HH) ribozyme [14,15]. Important viral specific protein–RNA interactions like HIV-1 Tat-TAR (*trans*-activating (Tat) response element) and Rev-RRE (Rev response element), which are crucial binding events in the HIV replication process, are competitively blocked by certain aminoglycoside antibiotics [16,17].

Given the vast therapeutic potential of RNA molecules, it is not surprising that several biophysical methods have been and are being developed to advance the understanding of RNA–protein, RNA–nucleic acid, and RNA–small molecule interactions, and hence, the discovery of potential small-molecule inhibitors that inhibit viral/bacterial-specific interactions. In particular, fluorescence-based methods, which utilize fluorescence properties such as fluorescence intensity (FI), fluorescence lifetime (FLT), and fluorescence polarization (FP), and fluorescence phenomenon like fluorescence resonance energy transfer (FRET) provide effective systems for examining such biological events, often in real-time and with great sensitivity.

Intrinsic fluorescence of nucleosides present in nucleic acids is very weak to be useful for any practical applications [18–20]. Excited-state lifetime measurements using fluorescence up-conversion with femtosecond time resolution reveal lifetimes in sub-picoseconds for the natural nucleosides, which virtually rules out any photophysical process in the excited state [21]. The synthetic explosion in the field of nucleoside chemistry has enabled the chemical biologist to overcome this limitation. Numerous structurally and photophysically diverse fluorescent nucleoside analogue probes have been developed and extensively applied in exploring nucleic acids structures, dynamics, and recognition events [22–28]. However, rational design and implementation of fluorescent ribonucleoside reporters in RNA-based biophysical assays still remains a challenge. In this review, we will provide a concise historical background on the development and applications of fluorescent nucleobase analogues. In particular, emphasis will be laid on the design and applications of base-modified fluorescent ribonucleoside analogues used as probes incorporated into RNA. Readers interested in the applications of fluorescent oligodeoxyribonucleotides are therefore suggested to find more details from various excellent reviews available in the literature [22–24,26–29].

PHOTOPHYSICAL PROPERTIES OF BASE-MODIFIED FLUORESCENT RIBONUCLEOSIDE ANALOGUES

Several design principles adopted to generate emissive nucleoside probes were either based on naturally occurring fluorescent heterocycles or fundamental physical organic chemistry, wherein, extending the Π conjugation in a ring system can potentially result in better photophysical properties [22–28]. Based on the size and hydrogen-bonding complementarities in comparison to natural nucleobases, base-mod-

ified nucleobase analogues can be broadly classified into the following categories: (a) size-expanded bases, (b) pteridines, (c) extended bases, (d) polycyclic aromatic hydrocarbon (PAH) base analogues, and (e) isomorphic bases. Size-expanded base analogues are those in which aromatic rings are either fused to pyrimidines or introduced between pyrimidine and imidazole rings. Such modifications usually render nucleosides highly fluorescent [28,29]. Pteridines are a class of naturally occurring bicyclic planar compounds, few of which are highly emissive and bear structural resemblance to the natural purines [24]. Extended base analogues are those in which known fluorophores (e.g., pyrene, phenanthroline, anthracene, bipyridine, terpyridine, etc.) are linked or conjugated to the bases via either a flexible or a rigid linker [28]. PAH base analogues are a class of nucleoside analogues in which the bases are replaced with fluorescent PAHs that are highly nonpolar and lack Watson–Crick (WC) hydrogen-bonding face [29]. The majority of size-expanded bases, pteridines, extended bases, and PAH base analogues studied are fluorescent deoxyribonucleosides, and, hence, their photophysical properties and applications will not be discussed in this review [22–24,26–29].

While most of the above-discussed nucleoside analogues structurally deviate from the natural bases significantly, isomorphic bases closely resemble the native bases with respect to their overall dimension and have the ability to form canonical WC base pairs (Fig. 1). An appealing feature of these isomorphic fluorescent ribonucleoside analogues is that they can be specifically positioned near the point of investigation in a target nucleic acid with minimum structural perturbations. Interestingly, only a few useful isomorphic analogues have been developed over the years. This is probably because the researchers working in this area have found it difficult to strike a balance between invoking isomorphicity and favorable photophysical properties. When the balance is shifted toward achieving isomorphicity, then the analogues most often show poor fluorescence properties, and vice versa.

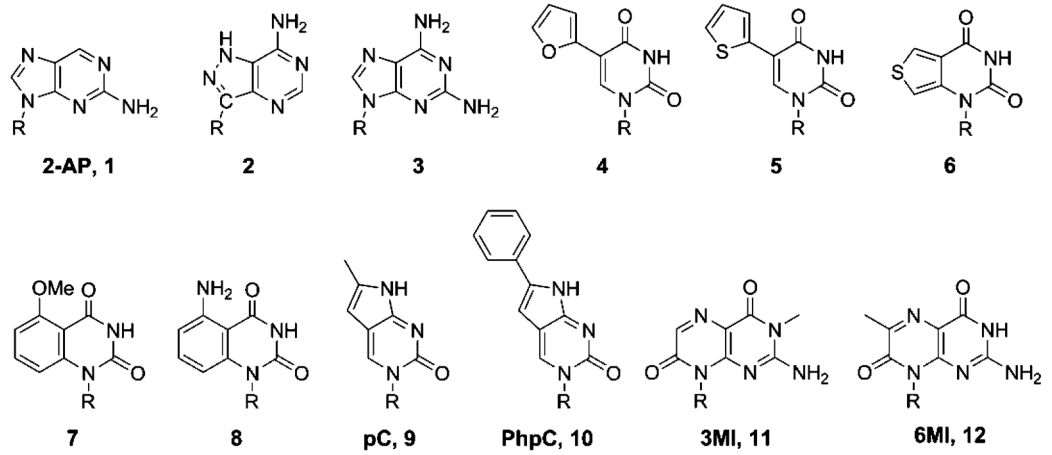

Fig. 1 Selected examples of isomorphic fluorescent ribonucleoside analogues (R = ribose).

2-Aminopurine (2-AP, **1**) ribonucleoside, which functions as an analogue of adenosine in base pairing and in several enzymatic reactions, is one of the most widely used fluorescent nucleoside analogues. Ward and co-workers have systematically studied the photophysical properties of adenosine analogues, 2-AP, formycin (**2**), and 2,6-diaminopurine (**3**) ribonucleosides [30]. In particular, 2-AP displays the following attributes characteristic of an useful nucleoside probe: (a) it forms stable WC-like base pairs with dT and U; (b) it shows strong emission at 370 nm when excited around 310 nm, a region that is far removed from the absorption maxima of natural bases and fluorescent aromatic amino acids; (c) it exhibits high quantum yield (Φ) of 0.68 in water; and (d) most importantly, its fluorescence is sensitive to changes in the polarity of its environment [31]. Several experimental studies complemented by

theoretical approaches explain the contrasting excited-state behavior of non-emissive adenosine and highly emissive 2-AP [20,32–36]. Unfortunately, the photophysical properties of adenosine analogues, formycin and 2,6-diaminopurine, were not very promising [30].

Akin to most other emissive analogues, fluorescence of 2-AP also is markedly quenched upon incorporation into oligonucleotides. This quenching phenomenon is sequence-dependent, and is mainly attributed to stacking interactions with the flanking bases [34,36–40]. Energy-transfer processes such as electron transfer, hydrogen-bonding interactions, and collisional interactions with neighboring bases also contribute to the overall quenching of fluorescence [31,36,37]. Because the fluorescence properties of 2-AP depends on the equilibrium between stacked and destacked states, and that this equilibrium can be altered by temperature, solvent, adjacent bases, and bound protein or small molecule, numerous biophysical assays have been developed to probe these scenarios using 2-AP [23,24,28]. Seela and coworker have reported the synthesis, base pairing, and fluorescence properties of oligonucleotides containing structural analogues of 2-AP, 7-deazapurine, and 8-aza-7-deazapurine [41]. While duplexes containing these modifications show stabilities comparable to that of duplexes containing 2-AP residue, their quantum efficiencies are significantly compromised.

Tor and co-workers have shown that a series of isostructural fluorescent nucleoside analogues can be generated by appending five-membered heterocycles at the 5- and 8-position of pyrimidines and purines, respectively [42–46]. Interestingly, pyrimidine and purine analogues exhibit contrasting photophysical behavior. While pyrimidine derivatives display two clear absorption maxima, one for the pyrimidine core and the other for the conjugated heterocycle (310–320 nm), purine derivatives show one major red-shifted absorption maximum around 300 nm [42,43,45,46]. Furan and thiophene-conjugated dT/U analogues display relatively low quantum yields (Φ = 0.01–0.035) as compared to furan-modified dA and dG (Φ = 0.69 and 0.57 for dA and dG, respectively). However, excellent correlations between emission energy and $E_T(30)$, Reichardt's microscopic solvent polarity parameter, were observed for furan- (**4**) and thiophene-conjugated (**5**) uridine analogues, suggesting that the modified pyrimidines are highly sensitive to changes in solvent polarity. These analogues were amenable to incorporation into DNA and RNA by chemical as well as by enzymatic methods. Their responsiveness to conformational changes within nucleic acids has been aptly utilized in monitoring abasic sites, and therapeutically relevant RNA–ligand and RNA–protein interactions [42,46–48].

In a similar venture, Tor and co-workers have developed fused thiophene analogues of uridine, and have studied their emission properties [45,49–51]. In particular, the isomorphic analogue (**6**), when excited at its absorption maximum (304 nm), results in a strong red-shifted emission corresponding to a quantum yield of 0.48 [49]. The efficacy of this analogue in positively signalling the presence of an RNA abasic site has been elegantly applied in developing a novel fluorescence-based assay for investigating the depurination activity of ribosome inactivating protein (RIP) toxins [50]. FRET pairs containing fluorescent nucleosides have been recently introduced by Tor and co-workers [52,53]. Expanded isomorphic uridine analogues based on 5-methoxyquinazoline-2,4(1*H*,3*H*)-dione (**7**) and 5-aminoquinazoline-2,4(1*H*,3*H*)-dione (**8**) effectively act as a donor for coumarin and an acceptor for tryptophan, respectively. Using these FRET systems, robust platforms were constructed to survey the binding of aminoglycoside antibiotics to the bacterial ribosomal decoding site and HIV Rev-RRE protein–RNA interaction [52,53].

The collection of useful isomorphic fluorescent ribonucleoside analogues has been expanded by the introduction of cytidine analogue, pyrrolo-C (pC, **9**) [54]. pC is significantly emissive with absorption and emission maximum at 350 and 460 nm, respectively. The quantum efficiency for the free nucleoside is around 0.2, which drastically drops to about 0.03 when placed opposite guanine residue in a duplex. Favorable properties such as isomorphicity, the ability to form a stable base pair with guanine, and the responsiveness of pC to changes in its microenvironment have made this analogue a promising probe for investigating the structure and dynamics of RNA. Recently, a few derivatives of pyrrolo-C (e.g., PhpC, **10**) have also been developed, which show better photophysical properties as compared to the parent fluorophore, pC [55–57].

METHODS TO INCORPORATE RIBONUCLEOSIDE ANALOGUES INTO RNA

Automated oligonucleotide synthesis is the method of choice to obtain site-specifically labeled RNA oligonucleotides. Although the synthesis of RNA oligonucleotides is essentially performed under the conditions employed for solid-phase DNA synthesis, RNA synthesis requires additional orthogonal protection of the 2'-OH group. Currently, there are three effective methods that are being commercially employed to synthesize oligoribonucleotides. Two methods use fluoride-labile *tert*-butyldimethylsilyl (TBDMS) or triisopropylsilyloxymethyl (TOM) protecting group at the 2'-OH position while an acid labile dimethoxytrityl (DMT) is used at the 5'-position [58–60]. RNA syntheses with TOM-protected phosphoramidite chemistry developed by Pitsch and co-workers are more efficient than synthesis with traditional 2'-O-TBDMS-protected phosphoramidites [59]. The third method uses a cyclododecyloxy-*bis*(trimethylsiloxy)silyl (SIL) protecting group at the 5'-OH position and the 2'-OH is protected with an acid-labile orthoester (ACE) group developed by Scaringe and Caruthers [61,62]. These methods are now being regularly used in synthesizing labeled oligoribonucleotides for bioanalytical and therapeutic applications [63]. However, numerous modified phosphoramidite substrates undergo degradation under the chemical conditions of solid-phase oligonucleotide synthesis, and during subsequent deprotection steps.

Alternatively, fluorescent RNAs can be obtained under very mild conditions by enzymatic incorporation of fluorescent ribonucleoside triphosphates using RNA polymerases, and by postsynthetic modifications [46–49,64–66]. Synthesis of many triphosphate substrates from their corresponding ribonucleosides does not involve strenuous protection–deprotection steps, and is usually performed using a conventional one-pot/two-step reaction developed by Ludwig [46–51,67,68]. Moreover, large quantities of RNA can be synthesized by transcription reaction with a minuscule amount of triphosphate substrate, and also, several modified transcripts can be obtained by manipulating the template sequence [46–49,51]. Despite these advantages, it is difficult to site-specifically label the nucleoside analogue by transcription reaction as there is no control over the site of incorporation in a transcription reaction. In addition, the modified triphosphate analogues are not always accepted and effectively incorporated into the growing RNA chain by polymerases [51]. In order to effect site-specific labeling by template-dependent enzymatic reaction, it is imperative to use a nucleoside pair that shows unique base pairing scheme as opposed to natural A·T and G·C pairs. For example, elaborate studies revealed that the triphosphates of isoguanosine (IsoG) and isocytidine (IsoC) can be effectively incorporated into nucleic acids by both DNA and RNA polymerases, albeit with compromised specificities [69]. Recently, Hirao and co-workers have reported site-specific incorporation of fluorescent ribonucleotides into RNA by transcription reaction using thienyl- and thiazolyl-based unnatural base pairs [70]. In another method, Micura and co-workers have site-specifically placed 2-AP in long oligoribonucleotides by enzymatically ligating two chemically synthesized shorter oligoribonucleotide strands containing 2-AP using T4RNA or T4DNA ligase [71,72].

APPLICATIONS OF BASE-MODIFIED FLUORESCENT RIBONUCLEOSIDES

RNA molecules fold into complex three-dimensional architectures, and undergo dynamic changes in conformation during recognition and binding processes [73,74]. Hence, environment-sensitive fluorescent ribonucleoside analogues that report these intricate dynamic and structural alterations in the form of changes in fluorescence properties have become powerful tools in investigating the structural and recognition properties of RNA. Here, we provide an overview of the applications of base-modified emissive ribonucleoside analogues designed to probe both intrinsic structural and binding properties of RNA. Notably, the majority of these applications use 2-AP due to its exquisite sensitivity to the microenvironment, high quantum yield, and commercial availability of 2-AP-modified RNA oligonucleotides [75]. However, the major shortcomings of 2-AP, emission maximum (~370 nm) and low quantum yield when incorporated into nucleic acids, significantly limit its applications to in vitro sys-

tems only. Over the years, several nucleoside analogues with diverse structures and photophysical properties have been reported, but only a few have been implemented in nucleic acids-based biophysical assays. Therefore, there is a huge demand for new nucleoside analogues with improved photophysical properties, which will also expand the scope of fluorescent nucleosides to in vivo systems. We have divided this section into two parts. In the first part, we give a brief account on the established fluorescence spectroscopy techniques, which make use of different properties of fluorescent ribonucleoside analogues. In the second part, we present a detailed discussion on the various applications of base-modified fluorescent ribonucleoside analogue probes.

Fluorescence techniques that use properties of fluorescent ribonucleosides

The fluorescence quantum yield, emission maximum, and excited-state lifetime are the most important properties that characterize a fluorescent molecule. Fluorescent molecules, which can report conformational changes, binding events, or enzyme activities by means of changes in the photophysical properties have become very useful tools in developing bioanalytical assays [76–78]. Base-modified fluorescent ribonucleoside analogues, which are going to be discussed in this section, report changes in their local environment via changes in their basic fluorescence properties such as quantum yield, emission maximum, and lifetime. Depending on the effects that a fluorescent analogue can produce owing to changes in its microenvironment, steady-state fluorescence (SSF) and or time-resolved fluorescence (TRF) spectroscopy techniques can be employed to investigate RNA structures, dynamics, and recognition events. Readers interested in the theoretical and technical details of these spectroscopy techniques are suggested to refer to literature reports [76–78].

Steady-state fluorescence (SSF) spectroscopy

SSF spectroscopy is a straightforward and widely employed technique. In this method the fluorophore is excited with a constant flow of photon and the emission profile is recorded. The emission profile essentially gives information regarding the energy maximum and quantum yield of the fluorophore in a given solvent system. Prior to emission, the excited-state energy can be affected by several factors such as solvent polarity, collisional interactions, temperature, pH and ionic strength, to name a few, which can potentially alter the emission maximum and/or the quantum yield [76]. Therefore, for fluorescent ribonucleoside analogues whose emission properties (λ_{em} and Φ) are sensitive to local environmental perturbations, SSF spectroscopy can be used to estimate the changes in these properties. For example, photophysical properties of 2-AP incorporated into oligoribonucleotides depend on the equilibrium between stacked and destacked states. When the 2-AP base is stacked with neighboring bases, its fluorescence is highly quenched, but when it is unstacked and solvent exposed, it shows remarkable enhancement in florescence [30,36]. Since this equilibrium can be affected by temperature, solvent, adjacent bases, and bound protein or small molecule, 2-AP can be used as a reporter to investigate the RNA folding and recognition processes. Similarly, several analogues listed in Fig. 2 that display excellent solvatochromism have been implemented in numerous fluorescence-based assays.

FRET is a photophysical phenomenon in which energy transfer takes place between two distinct chromophores commonly known as donor and acceptor [76]. The efficiency of the energy-transfer process depends on the extent of overlap between donor emission band and acceptor absorption band and the distance between the donor–acceptor pair. Most FRET-based studies use steady-state measurements in which changes in FI of the donor or acceptor are measured. Although several FRET-based systems have been designed using typically large donor–acceptor pairs to investigate RNA folding dynamics and binding events, donor–acceptor pairs made of nonperturbing nucleoside surrogates are rare. Wilhelmsson and co-workers for the first time assembled a FRET pair using 1,3-diaza-2-oxophenoxazine (tC^o) as the donor and 7-nitro-1,3-diaza-2-oxophenothiazine (tC_{nitro}) as the acceptor [79]. More recently, Tor and co-workers have developed a uridine analogue, 5-aminoquinazoline-2,4(1*H*,3*H*)-dione

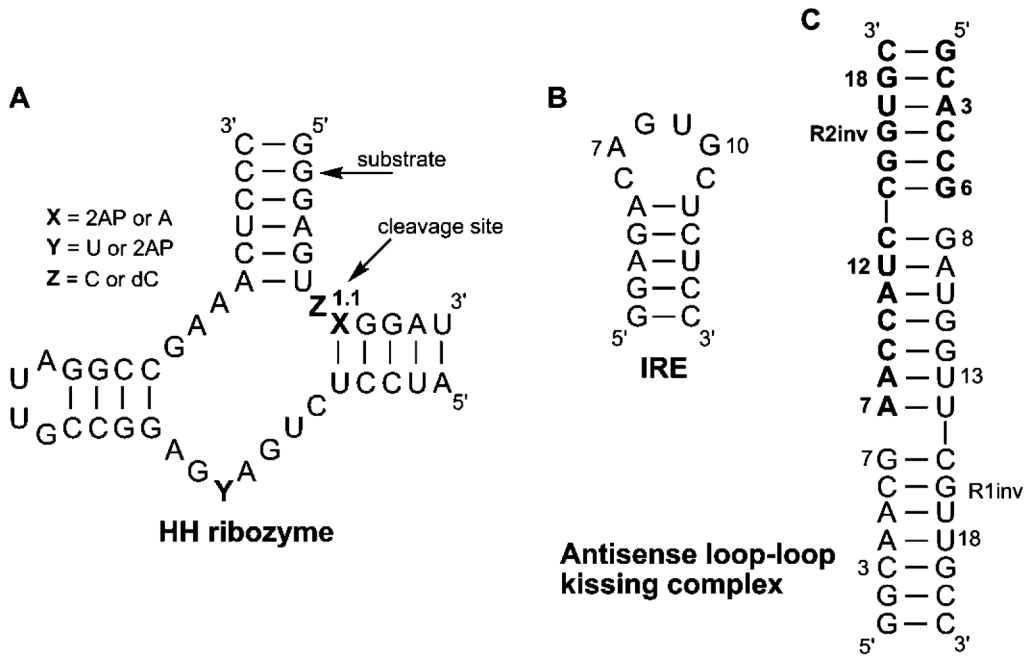

Fig 2. (A) Sequence of *trans*-cleaving ribozyme and its RNA substrate [88,91]. (B) Secondary structure of the human IRE RNA hairpin motif. Nucleosides A7 and G8 have been individually replaced with 2-AP [99]. (C) Base pairing scheme of the loop–loop "kissing" complex formed between *ColE1*plasmid-encoded RNA I and RNA II transcripts (so-called R1inv and R2inv). The R2inv sequence is depicted in bold capitals. A3 and A8 of R2inv and A9 of R1inv have been replaced with 2-AP [100].

(**8**), which acts as an acceptor for tryptophan. Using this FRET pair, they studied the binding of viral Rev peptide to RRE [53].

Many fluorescent molecules upon excitation with polarized light yield polarized emission, which can also be described in terms of anisotropy (FA). The extent of FP depends on the rate of rotational diffusion during the lifetime of the excited state, which in turn is dependent on the viscosity of the solvent, the size, the shape, and the inherent flexibility of the tumbling molecule [76]. Although FA measurement has been widely applied in investigating the dynamics and the complex formation of various proteins, it has been sparsely utilized in nucleic acids studies [80,81]. For accurate measurement of anisotropy, the fluorophore once incorporated into oligoribonucleotides should exhibit reasonable quantum yield and lifetime comparable to the rotational correlation times of the oligoribonucleotides. In particular, nucleoside analogues 6MI, tC^o, and pC show properties that are suitable for FP-based experiments. Using the FA of pC, Walter and co-workers devised an assay to distinguish an ssRNA from a dsRNA. While free pC ribonucleoside shows a very low anisotropy (0.06), the anisotropy of pC incorporated into ssRNA and dsRNA increases by 2- and 3-fold, respectively [82]. In a recent study, Herschlag and co-workers have used 6MI as a FP probe to study the nanosecond dynamics of the RNA helix [81,83]. They measured the anisotropy of 6MI-labeled model duplexes containing one or two helices connected by different junctions. The anisotropy was found to be higher for constructs containing a long helical region as compared to constructs containing two helices connected by various linkers. These results suggest that an RNA containing short helical regions connected by single-stranded segments is more flexible than an RNA containing a long helical region.

Time-resolved fluorescence (TRF) spectroscopy

TRF spectroscopy is a powerful technique that is used for measuring intensity decay profiles and excited-state lifetimes of fluorophores. Time-resolved measurements can provide insight into the dynamics of the excited state and decay kinetics of fluorophores. Unlike steady-state measurements, time-resolved measurements can be used to distinguish between individual species present in a heterogeneous population based on their lifetime. The heterogeneity can arise owing to the presence of different conformational states of a given fluorophore. For example, intensity decay kinetics of 2-AP nucleoside is monoexponential, corresponding to a lifetime of ~10 ns [30]. However, when incorporated into oligodeoxyribonucleotides it exhibits four distinct lifetimes ranging from 50 ps to 8 ns [84,85]. The longest lifetime has been assigned to the unstacked 2-AP base, whereas the shortest lifetime has been attributed to the completely stacked state. Importantly, the distribution of 2-AP's stacked and unstacked states can be changed by solvent, temperature, and neighboring bases, and by bound proteins, nucleic acids, and small molecules. Hence, 2-AP lifetimes can be used to assess changes in conformational states that take place during a folding or binding process. Applications of fluorescent ribonucleoside analogues that report changes in conformation or binding event via changes in quantum yield, lifetime, or decay kinetics will be discussed in detail in the following section.

RNA structure and dynamics

The fluorescence of 2-AP within nucleic acids is known to be predominantly quenched via a complex excitation energy transfer and charge-transfer processes, which greatly depend on the extent of stacking between 2-AP and neighboring bases [34,36–40,86]. Therefore, capturing these dynamic processes can provide direct information on the stacking interactions. The suitability of 2-AP as a probe for monitoring conformational changes in RNAs was independently demonstrated by two groups. Adamiak and co-worker have studied the dynamics of RNA bulge loop conformations using 2-AP labeled RNAs [87]. Thermal melting data and thermodynamic parameters indicate that a bulge in RNA duplexes leads to destabilization of regular helix structure. Their results also indicate that the structural properties of RNA bulge loops containing either 2-AP or adenosine are similar, which strongly favors the use of 2-AP as a nonperturbing conformational probe. Porschke and co-workers have studied the topology of the HH ribozyme dynamics by measuring the changes in fluorescence of 2-AP riboside incorporated either in the substrate or in the ribozyme (Fig. 2) [88]. Complex formation between the substrate containing 2-AP near the cleavage site and the *trans*-cleaving ribozyme in the presence of Mg^{2+} resulted in 2.5-fold fluorescence enhancement, indicating the formation of a less stacked structure around 2-AP in the complexed state. However, when ribozyme containing 2-AP at a position away from the cleavage site was annealed to an unmodified substrate, a decrease in fluorescence associated with a stacked state around the 2-AP was observed. In order to investigate the role of Mg^{2+} in the catalysis, several ribozyme constructs containing 2-AP modification at various sites were synthesized. Binding constants in the range of 7600 M^{-1} down to 12 M^{-1} were measured, suggesting the presence of multiple Mg^{2+} binding sites in the ribozyme with varying affinities. The dynamics of the ribozyme was also analyzed by fluorescence-detected temperature jump relaxation in the presence of metal ions. In this study, the equilibrium state of the ribozyme was disrupted by suddenly increasing the temperature by a few degrees, and the relaxation process was monitored by recording the changes in 2-AP fluorescence as a function of time. Relaxation time constants determined for ribozymes substituted at different positions were found to indicate both global and local conformation changes over a broad time range [89]. Base stacking dynamics in GNRA-type hairpin loop structures, which are abundant in natural RNAs, have also been studied using 2-AP fluorescence and fluorescence-detected temperature jump relaxation methods [90]. They have used two tetramer sequences, G**2AP**AA (HP1) and GA**2AP**A (HP2), containing 2-AP in the loop region. The 2-AP fluorescence of HP1 has been found to be significantly higher as compared to HP2, suggesting a less stacked environment around 2-AP in HP1. Temperature jump relaxation process

monitored using 2-AP fluorescence revealed a relaxation process with a time constant of 22 μs for HP1, whereas HP2 showed two relaxation processes corresponding to time constants, 5 and 41 μs. These results clearly demonstrate the existence of more than one conformational state that could not be identified by NMR analysis.

Tor and co-workers have used an HH ribozyme substrate modified at position 1.1, a position adjacent to the cleavage site, with 2-AP as a real-time probe for studying the enzymatic cleavage and inhibition of a *trans*-active HH ribozyme (Fig. 2) [91]. 2-AP in the ribozyme-substrate complex is stacked and hence shows low fluorescence. However, as the ribozyme-mediated cleavage of the 2-AP-modified substrate proceeds, a continuous increase in FI is observed owing to dissociation of the cleaved substrate from the complex. The kinetic parameters determined by fluorescence and radioactive labeling methods were in good agreement. Using this fluorescence assay, three new inhibitors of HH ribozyme, neo-acridine, guanidinoneomycin B, and $[\Delta\text{-(Eilatin)Ru(bpy)}_2]^{2+}$, which block the cleavage reaction, were identified.

Walter and co-workers have used 2-AP as a site-specific probe to study structure–function relationships in the hairpin ribozyme, a small endonucleolytic RNA motif [92]. In order to monitor the structural changes taking place around the cleavage site, the conserved substrate base U+2 located near the core of the docked ribozyme-substrate complex has been replaced with 2-AP. Upon complex formation, more than a 100 % increase in fluorescence has been observed, indicating a local structural reorganization associated with better domain docking and unstacking of +2 base. 2-AP-incorporated nucleic acids display four distinct FLTs [84,85]. While the longest lifetime component (~8 ns) corresponds to a completely unstacked base, the shortest lifetime (~50 ps) corresponds to a strongly stacked base. During domain docking, a substantial shift toward the longest lifetime component is observed, which further corroborates the notion that +2 base unstacks upon complex formation.

In another study, a combination of 2-AP fluorescence and FRET was used to monitor the local conformational changes in the catalytic core of the *trans*-acting hepatitis delta virus ribozyme (HDV) [93]. HDV is a human pathogen that uses a catalytic RNA motif to process its genome. The crystal structure of the ribozyme shows a cytosine residue (C75) located near the 5'-OH leaving group, which acts as a general acid/base in hydrolyzing the phosphate backbone [94]. Walter and co-workers have constructed a fluorescent *trans*-acting HDV ribozyme by replacing G76 with 2-AP. While 2-AP fluorescence is strongly quenched in the ribozyme-substrate complex, the product complex upon substrate cleavage displays significantly enhanced emission, consistent with the destacked and solvent exposed 2-AP base [93]. Woodson and co-workers have studied the folding kinetics of 2-AP-labeled *Azoarcus* group I ribozyme by employing stopped-flow fluorescence spectroscopy [95]. Early results obtained using time-resolved footprinting experiments revealed that the ribozyme rapidly folded into its native tertiary structure ($\tau < 30$ ms) in the presence of Mg^{2+}. However, when stopped-flow methods were used, the modified ribozyme exhibited two equilibrium folding transitions as a function of Mg^{2+} concentration and four kinetic folding transitions with observed rate constants of 100, 34, 1, and 0.1 s^{-1}.

Zewail and co-workers have shown that 7-deazaguanine quenches the fluorescence of 2-AP on a 1 ps time scale, which is much faster than those observed for all natural bases [96]. Drawing inspiration from this report, Xia and co-worker designed a series of GNRA tetraloops labeled with 2-AP and 7-deazaguanine next to each other, and investigated the intrinsic stacking dynamics of RNA by femtosecond time-resolved spectroscopy [97]. Based on femtosecond dynamics probing and other reports, a dynamic multiconformation model composed of an ensemble of conformations was proposed for GNRA tetraloop motif. In a similar approach, solvent accessibility of 2-AP-labeled RNA stem-loop constructs was estimated using acrylamide fluorescence quenching to gain insight into local RNA structure and dynamic features [98].

The iron responsive element (IRE) is a short hairpin-loop RNA motif containing six phylogenetically conserved nucleotides (C6A7G8U9G10C11), which is sequence-specifically recognized by IRE-binding protein when the protein is devoid of 4Fe-4S cluster. Hall and Williams used temperature-dependent SS and TRF methods to map the structure and dynamics of the IRE loop [99]. They con-

structed 2-AP-modified IRE loops, in which two purine nucleotides (A7 and G8) in the loop were individually replaced with 2-AP (Fig. 2). While IRE containing 2-AP at position 7 exhibited an increase in fluorescence with an increase in temperature (4–35 °C), 2-AP at position 8 displayed fluorescence quenching with an increase in temperature. The longest lifetime component of 2-AP at position 8 corresponding to a destacked base was found to vary between ~8.7 ns (5 °C) and ~5.0 ns (35 °C). A similar trend was also observed for the IRE-containing 2-AP at position 7. However, the shortest lifetime component, which corresponds to a stacked state, revealed a 2-fold longer lifetime for IRE labeled at position 8 as compared to IRE labeled at position 7. The results obtained from these experiments indicate a flexible 2-AP at A7, moving between stacked and unstacked positions, while 2-AP at G8 is predominantly exposed to solvent.

The sensitivity of 2-AP to conformational changes has been elegantly used to study the equilibrium and real-time kinetic pathway for the association of naturally occurring antisense RNA hairpins derived from *ColE1*, a bacterial plasmid [100]. In *ColE1*, the plasmid-encoded RNA II transcript forms a stable hybrid with template DNA near the replication origin, which upon cleavage by RNaseH results in primer formation [101]. The primer formation and the subsequent plasmid replication are kinetically repressed by the formation of a hybrid between RNA II and an antisense RNA I transcript. Marino has studied the multistep folding pathway for the binding of RNA I and RNA II using fluorescence-detected stopped-flow and equilibrium methods [100]. In their study, the formation of loop–loop "kissing" complex intermediates between the RNA hairpins (so called R1inv and R2inv, derived from RNA I and RNA II transcripts, respectively) substituted with 2-AP at positions in the complementary loops were established by monitoring the changes in 2-AP fluorescence (Fig. 2). The complex formation resulted in a 5–10-fold fluorescence quenching, which provided a sensitive means to determine the equilibrium binding properties. Results obtained from stopped-flow experiments clearly indicated at least three different microenvironments around the 2-AP probes during association of RNA hairpins.

Pyrene-modified nucleic acids have been widely used in several biophysical assays because its fluorescence is highly sensitive to its hydrophobic microenvironment [102–105]. Kim and co-workers have synthesized pyrene-conjugated RNA constructs by automated RNA synthesis, and have studied the dynamics of RNA bulge conformations using HIV-I TAR RNA as a model system [106]. TAR contains a conserved bulge site made of U23C24U25, which specifically interacts with arginine-rich Tat peptide, a critical protein factor necessary for viral replication (Fig. 3). Site-specifically modified TAR constructs containing base-modified pyrene U23 (P23-TAR) and U25 (P25-TAR) were used to study the changes in conformation upon addition of a Tat peptide mimic, argininamide. While addition of argininamide to P25-TAR resulted in a remarkable 6-fold increase in fluorescence, P23-TAR displayed only a marginal enhancement in fluorescence. These observations clearly reveal that the pyrene-attached U25 base undergoes considerable conformational change, namely, from a stacked to an unstacked state upon complex formation. Subsequent CD studies and ab initio calculations based on self-consistent reaction field also revealed a reoriented and less stacked U25 base projected outside the RNA groove in the bound state. These results were consistent with modeling studies performed on the natural RNA under unbound and bound conditions [106]. One or two fluorescent ethynylpyrenes, substituted at C2 position of adenine base, were introduced into a series of short RNA duplexes by following orthoester chemistry with the intention to probe the dynamics of RNA folding [107]. A relationship between the flanking bases and the propensity of the pyrene moiety to intercalate was established by monitoring temperature-dependent pyrene fluorescence. The presence of flanking G-C pairs clearly favored the intercalation of pyrene chromophore into the duplex, which resulted in significant fluorescence enhancement. On the other hand, flanking A-U pairs partially prevented the intercalation process. Tanaka and Okamoto developed a fluorescence assay to detect RNA poly(A) tracts by employing a pyrenecarboxamide-tethered oligodeoxynucleotide [108]. The probe oligonucleotide hybridized to the target RNA containing poly(A) tract positively signaled the presence of poly(A) tract with significant fluorescence enhancement.

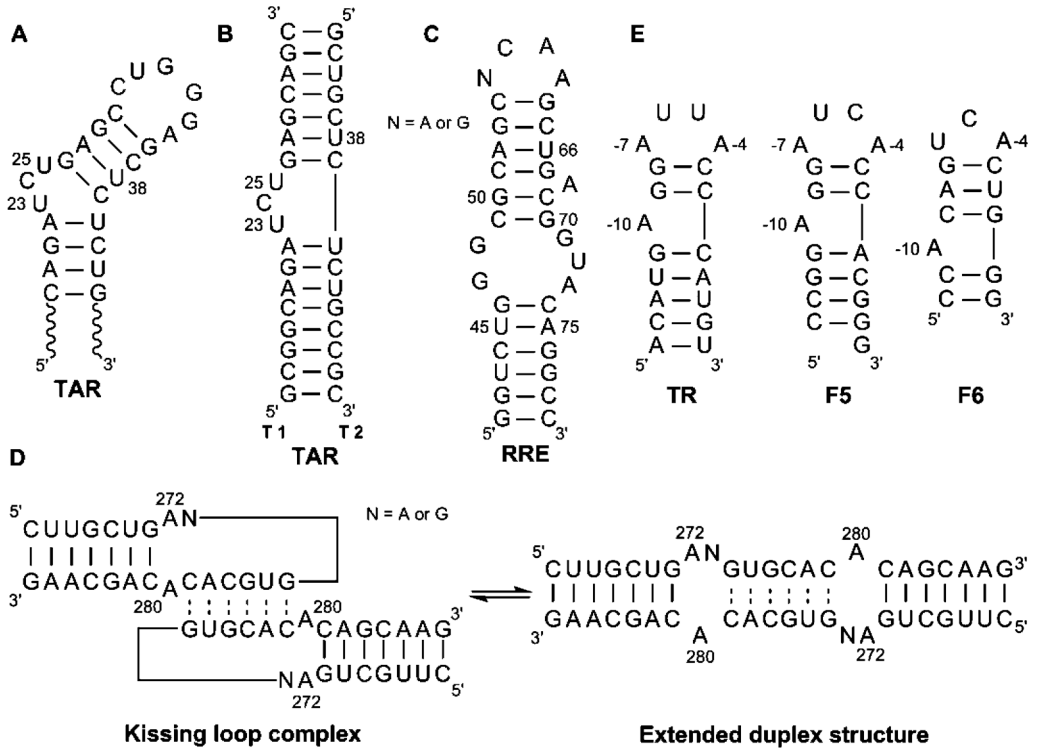

Fig 3 (A) Core sequence of HIV-1 TAR RNA used in several studies. Kim has used TAR RNA constructs containing pyrene-labeled uridine at U23, U25, and U31 [106]. In another study, nucleosides C24 and U25 have been substituted with 2-AP [123]. (B) TAR RNA duplex assembled using T1 ssRNA containing furan-conjugated uridine (**4**) at U23 and U25, and complementary ssRNA, T2 [48]. (C) Sequence of HIV-1 short stem-loop RRE surrogate RNA construct. Marino has replaced A68 and U72 with 2-AP [121], and Tor has incorporated fluorescent uridine analogue (**8**) at U66 [53]. (D) Schematic representation of the structural conversion of the HIV DIS loop–loop kissing complex to extended duplex conformation. Tor and co-workers have incorporated 2-AP at positions 272 and 280, and have studied the DIS-aminoglycosides interactions [131]. (E) Sequence of the MS2 RNA translation operator (TR), F5 aptamer family and F6 aptamer family, respectively. -4A, -7A, and -10A bulge residues in TR, F5, and F6 were individually replaced with 2-AP [113].

pC as a free nucleoside is highly emissive, but when incorporated into ssRNA, a drastic quenching in fluorescence is observed. The fluorescence is further quenched in an RNA duplex [82]. The utility of pC as an RNA conformational probe was initially demonstrated by Walter [82]. In this study, a single-stranded RNA containing pC was used to measure the kinetics of association and dissociation of an RNA/DNA duplex by monitoring the changes in pC fluorescence. Hou and co-workers have enzymatically replaced a cytidine residue with pC of a highly conserved and structurally dynamic C74C75A76 sequence at the 3'-end of a mature tRNA [109]. The $tRNA^{Cys}$ up to C74 was synthesized by in vitro transcription reaction, and pC and adenosine were then incorporated at positions 75 and 76, respectively, by using CCA-adding enzyme in the presence of respective triphosphates. Stopped-flow fluorescence spectroscopy was then used to investigate the kinetics of translocation of labeled tRNA from A to P site. Time course experiments revealed a two-phase reaction, with an initial increase in FI (k_{app} = ~19 s^{-1}) followed by a decrease in FI (k_{app} = ~4 s^{-1}). The rate constants were found to be in consensus with the rates obtained with unmodified tRNA by other biophysical methods. Together, these experiments underscore the potential usefulness of pC as a probe for monitoring RNA structure and functions.

RNA–protein and RNA–small molecule interactions

RNAs perform numerous functions in prokaryotes, eukaryotes, and in many viruses mostly by interacting with proteins and small molecules. RNAs form complex secondary and tertiary structures such as stem-loops, bulges, and pseudoknots, and often these features are preferentially identified by proteins and small molecules [1–3]. In particular, RNA motifs that regulate enzyme activity, gene expression, and interact with viral and bacterial proteins or small-molecule metabolites are being intensely investigated as therapeutic targets [9,12,110–112]. Needless to say, 2-AP-modified RNA constructs have been extensively utilized in estimating these interactions [23,75]. However, new fluorescent nucleoside analogues with favorable photophysical properties have been developed and implemented in biophysical assays to advance the understanding of RNA–protein and RNA–small molecule interactions [28].

Stockley and co-workers have probed the dynamics and kinetics of complex formation between bacteriophage MS2 coat protein and two in vitro evolved RNA aptamers by site-specifically replacing key adenosine residues with 2-AP [113]. In this study, the ability of 2-AP in reporting the stacked and destacked states has been utilized to compare the conformational dynamics of the wild-type RNA translational operator (TR) and two aptamers (F5 and F6). A series of oligoribonucleotides of the 19-mer TR, 18-mer F5 aptamer, and 14-mer F6 aptamer were chemically synthesized in which -4A, -7A, and -10A bulge residues were individually replaced with 2-AP (Fig. 3). Upon the addition of saturating concentration of MS2 coat protein to -4TR and -4F5 constructs, an enhancement in 2-AP fluorescence was observed. However, protein binding to -4F6 produced only a marginal change in 2-AP fluorescence. While FI of all the oligoribonucleotides containing 2-AP at -7 position was found to be quenched, FI of constructs containing 2-AP at -10 position was found to be significantly enhanced. The observed increase as well as decrease in fluorescence intensities as a function of position was found to be consistent with the stacked and destacked state of the adenosine residues in the X-ray structure of a known MS2 protein-RNA complex. Furthermore, the X-ray structure of MS2 protein-RNA complex and fluorescence data obtained using the wild-type TR, a natural target for coat protein, show strikingly similar conformational dynamics for synthetic aptamer-protein and wild-type RNA-protein complexes.

N proteins from bacteriophages (λ, P22, and Φ21) containing N-terminal arginine-rich peptide sequences regulate transcription elongation by binding to their cognate nascent "boxB" mRNA hairpins. The sequence specificity of N-terminal arginine-rich peptides for "boxB" hairpins among related bacteriophages has been recognized as an excellent system for studying protein–RNA interactions [114]. Roberts and co-workers have constructed synthetic "boxB" RNA hairpins labeled with 2-AP in the bulge region and a series of peptides (11–22 residues) based on the N protein binding domains. They have analyzed the binding affinities and specificities of the peptide-RNA complexes by monitoring 2-AP fluorescence quenching as a function of peptide concentration [115]. Fluorescence measurements indicate that λ and P22 N peptides bind their RNA targets with high specificity and equal affinities. However, peptides derived from Φ21 showed poor specificity for their targets. In another report, Hall has studied the structure and dynamics of the polyadenylation inhibition element (PIE) RNA when free and bound to U1A protein, a component of the eukaryotic pre-mRNA processing complex, by using time-resolved FRET and 2-AP fluorescence [116]. PIE, located at the 3'-end of the pre-mRNA, adopts a U-shaped structure, thereby providing binding sites for a single U1A protein. In this study, model PIE oligoribonucleotides containing 2-AP in the stem and loop regions were chemically synthesized. Lifetime measurements clearly indicate that the 2-AP in the stem region is stacked in the free oligoribonucleotide and also remains stacked when bound to the protein. However, 2-AP in the bulge region is stacked when free, but gets unstacked upon binding to the protein, which is consistent as this nucleoside is directly involved in the binding event.

Li and co-workers have used a noninvasive 2-AP fluorescence assay to study the pseudouridylation of a specific uridine to its C-glycosyl isomer (pseudouridine) by H/ACA small nucleolar ribonucleoprotein particles (H/ACA RNPs) [117]. H/ACA RNPs are multicomponent enzymes made up of four core proteins (Cbf5, Gar1, Nop10, and L7Ae/NHP2) [118]. The enzyme complex uses a small non-

coding RNA as guide sequence to capture the RNA substrate for pseudouridylation of a specific uridine residue. In their study, a model RNA substrate containing 2-AP next to the target uridine residue was annealed with the guide RNA and then incubated with a trimeric protein complex (Cbf5-Nop10-Gar1) to allow the formation of RNP. Conformational changes occurring during the docking of the substrate near the catalytic residue (Cbf5) were studied by monitoring the changes in 2-AP fluorescence as a function of increasing concentrations of L7Ae protein. L7Ae titration showed significant increase in fluorescence, indicating an L7Ae-induced conformational change near the target uridine [117]. Results obtained through X-ray crystallography and fluorescence spectroscopy prompted Li and co-workers to conclude that the pseudouridylation requires the reorganization of guide RNA by L7Ae, assisted by trimeric protein complex, to recruit the target uridine at the active site [119].

Rev, a HIV-1 regulatory protein that interacts with Rev responsive element (RRE) RNA motif within the *env* gene, plays an important role in transporting unspliced or partially spliced mRNAs from the nucleus to the cytoplasm [120]. Since Rev-RRE complex formation is essential for viral replication, several biophysical methods have been developed to investigate the structure and kinetics of this complex formation, and hence, the discovery of new drug therapies against HIV-1 infection [16]. Marino and co-workers have selectively incorporated 2-AP into a short stem-loop RRE surrogate RNA sequence in nonperturbing positions (A68 and U72), and studied the binding of Rev peptide and aminoglycoside ligands by fluorescence method (Fig. 3) [121]. Upon binding to Rev peptide, RRE-72AP exhibited a 2-fold fluorescence enhancement corresponding to a binding constant in nanomolar range (~20 nM). Furthermore, stopped-flow fluorescence kinetic measurements revealed a two-step process involving diffusion-controlled binding event, followed by isomerization of the RNA. Utilizing fluorescent RRE-68AP and -72AP constructs, three classes of binding sites (noninhibitory, competitive, and nonspecific) for neomycin were identified [121]. In a subsequent report, Marino and co-workers used the above-discussed fluorescence method to identify drug-like molecules from a limited screen of small heterocyclic compounds. Out of this focused screen, proflavine has been found to specifically bind RRE with high affinity and competitively inhibit the formation of Rev peptide-RRE complex [122]. Recently, Tor and co-workers identified a new FRET pair in which 5-aminoquinazoline-2,4(1*H*,3*H*)-dione (**8**), an uridine analogue, acts as an acceptor for tryptophan. To demonstrate the utility of this FRET pair, they studied the binding of Rev peptide to fluorescently modified RRE (Fig. 3). When the Rev-RRE complex was excited at the absorption maximum (280 nm) of tryptophan, a decrease in tryptophan emission at 350 nm and an increase in acceptor emission at 440 nm were observed. Binding constants determined using Rev-RRE titration curves were found to be in good agreement with the previously reported values [53].

Binding of a 24-residue arginine-rich peptide derived from HIV Tat protein and neomycin to HIV-1 TAR have been characterized by using a truncated TAR sequence modified with 2-AP in the bulge region (C24 and U25, Fig. 3). Peptide and neomycin binding to 2-AP-labeled TAR constructs resulted in substantial fluorescence enhancement, indicating a destacked environment around 2-AP upon complex formation [123]. The results obtained using SSF were consistent with the solvent-exposed 2-AP as observed in NMR studies of the complex. Tor and co-worker have reported the enzymatic synthesis of fluorescently labeled TAR constructs, and have studied their interaction with the Tat peptide [48]. A duplex TAR construct containing the bulge sequence (binding domain), but lacking the loop segment was assembled by annealing a fluorescent T1 strand and an unmodified complementary T2 strand (Fig. 3). The fluorescent T1 strand was synthesized by incorporating an emissive and microenvironment-sensitive furan-conjugated uridine triphosphate into the bulge region (U23 and U25) by transcription reaction. A saturable binding isotherm corresponding to 50 % reduction in fluorescence was observed upon addition of increasing concentrations of Tat peptide to TAR duplex. Recently, Maiti and co-workers performed a thorough thermodynamic analysis of a 2-AP-incorporated TAR and Tat complex by using calorimetric, spectroscopic, and osmotic stress methods [124].

The dimerization initiation site (DIS) of HIV-1 genomic RNA is an attractive, yet underutilized, viral RNA target for antiretroviral therapy [125]. This highly conserved stem-loop structure composed

of a self-complementary hexanucleotide sequence initiates the dimerization of the genomic RNA by forming an intermediate kissing-loop complex between the loops. The kissing-loop complex is further rearranged into a stable extended duplex isoform by nucleocapsid protein (NCp7) as part of the viral maturation process [126]. It has also been shown that deletion or mutation of the DIS results in a dramatic decrease in the rate of viral replication [127]. By replacing one of the six nucleotides in the loop region of DIS with 2-AP (DIS-2AP), Marino and co-workers have unequivocally distinguished the two DIS dimer isoforms, namely, the kissing-loop complex and the stable extended duplex (Fig. 3) [128]. Titration of DIS-2AP hairpin with complementary DIS in the presence of divalent cations resulted in 6-fold quenching in 2-AP FI. The decrease in FI has been attributed to the formation of 2-AP·U base pair in the DIS kissing loop–loop helix, wherein the 2-AP is significantly stacked. Packaging sequence (Ψ-site, ~120 nt) derived from HIV-1 genome has been selectively labeled with 2-AP at the DIS stem loop by ligating two long RNA fragments, and the conformational changes incurred during the dimerization process have been studied using 2-AP fluorescence [129]. X-ray crystal structures show remarkable structural resemblance between HIV DIS complex and bacterial decoding site complexed with paromomycin [125]. Analogous to bacterial A-site, which contains conformationally flexible adenosine residues, DIS kissing-loop and extended isoforms also contain flexible A272 and A273 (Fig. 3). Crystal structures of DIS-aminoglycoside complexes show that A272 and A273 residues are extrahelical in the bound state [130]. Drawing inspiration from these observations, Tor and co-workers designed two 2-AP-modified hairpin DIS RNA constructs, AP272 and AP273 (Fig. 3) [131]. Binding of paromomycin and neomycin to AP272 RNA resulted in significant fluorescence enhancement, whereas ligand binding to AP273 RNA resulted in fluorescence quenching. Binding isotherms obtained by monitoring the changes in fluorescence as a function of ligand concentration yielded submicromolar EC_{50} values for paromomycin and neomycin.

Deleterious effects of aminoglycoside antibiotics emanate from their ability to induce conformational changes in the bacterial ribosomal decoding site (A-site), which involves the destacking of A1492 and A1493 residues [13]. This pre-organization of A-site in the presence of aminoglycosides reduces the energetic cost required to discriminate the cognate codon-anticodon interaction, and hence, lowers the fidelity of translation [132]. Conformational flexibility of the adenosine residues (A1492 and A1493) in the A-site has been extensively exploited in designing several 2-AP-based fluorescence assays to characterize the energetics and dynamics of aminoglycoside-induced conformational changes in the A-site of rRNA [133]. Several groups have assembled fluorescent A-site RNA surrogates by replacing A1492 or A1493 with 2-AP, and have determined the binding constants of A-site-aminoglycosides complexes by monitoring the changes in 2-AP fluorescence (Fig. 4) [134–137]. Hermann and co-worker used fluorescent pteridine analogues 3-methylisoxanthopterin (3MI) and 6-methylisoxanthopterin (6MI), which display higher quantum efficiencies and red-shifted emission maxima, as alternatives to 2-AP to investigate the conformational changes in the decoding site triggered by ligand binding (Fig. 4) [138]. In this study, A1493 has been replaced with either 3MI or 6MI to generate A-site oligoribonucleotide constructs. Tobramycin and paromomycin induced concentration-dependent fluorescence quenching in both 3MI- and 6MI-modified A-site constructs. The EC_{50} values determined using 3MI and 6MI for tobramycin and paromomycin binding to A-site were found to be in good agreement with the results obtained using a 2-AP-labeled A-site RNA.

Tor and co-worker synthesized model fluorescent A-site RNA by site-specifically incorporating furan-conjugated uridine triphosphate at U1406 by transcription reaction (Fig. 4) [46]. This microenvironment-sensitive fluorescent probe promptly reports the binding of paromomycin and neomycin to A-site construct. Intriguingly, 2-AP-modified A-site constructs have failed to detect neomycin binding to A-site. This observation is particularly perplexing as the crystal structures of A-site complexed with paromomycin and neomycin show close resemblance [139]. In order to address this issue, Tor and co-worker assembled an A-site RNA duplex composed of furan-conjugated uridine at 1406, which emits at 430 nm and 2-AP at 1492, which emits at 370 nm [46]. When titrated with neomycin, the doubly labeled A-site effectively detected the binding event with significant fluorescence enhancement cor-

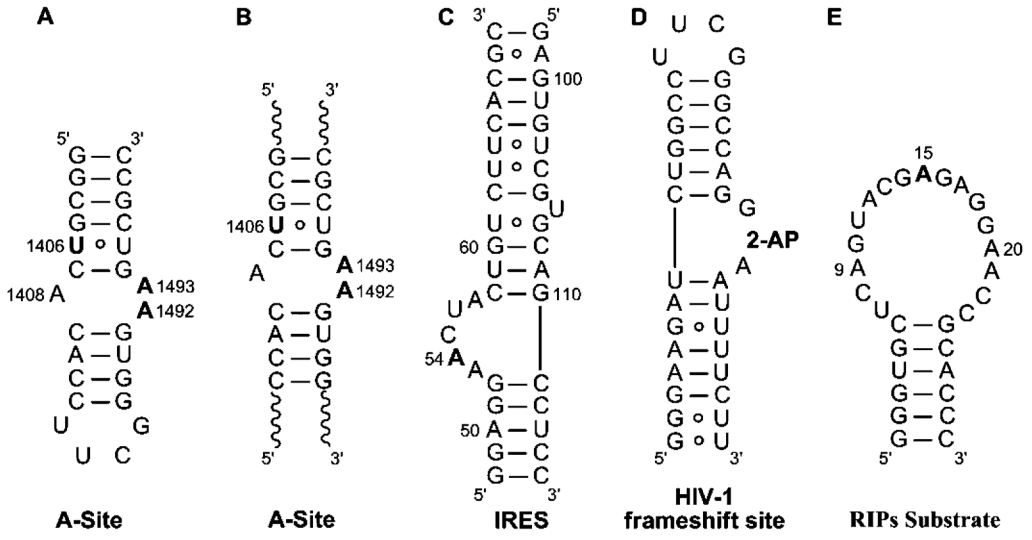

Fig. 4 (A) and (B) Sequence of bacterial decoding-site RNA constructs. Nucleoside positions A1492, A1493, and U1406 have been replaced with fluorescent probes such as 2-AP, furan-conjugated uridine (**4**), and pterdines [46,52,134–138]. (C) Secondary structure of the IRES subdomain IIa. A54 has been replaced with 2-AP [143]. (D) Truncated frameshift site RNA construct, and a 2-AP substituted for the central guanosine in the three-purine GGA bulge [144]. (E) α-sarcin/ricin hairpin RIPs RNA substrate. A15 is specifically depurinated to generate an abasic site by RIP toxins such as ricin and saporin [50].

responding to the emission maximum of furan-modified uridine, while there was a very minimal change in fluorescence corresponding to 2-AP emission maximum. Together, these observations clearly point out that 2-AP at 1492 does not hamper the binding of neomycin to A-site. Hence, 2-AP does not always function optimally. Recently, a FRET-based displacement assay has been developed for real-time monitoring of RNA–small molecule interaction [52]. In this study, a 5-methoxyquinazoline-2,4(1*H*,3*H*)-dione-based emissive uracil analogue (**7**) has been used as a donor for coumarin-modified aminoglycoside antibiotic acceptors. The uracil analogue was site-specifically incorporated into an A-site stem-loop RNA construct at U1406 position. Upon titrating coumarin-labeled aminoglycosides into fluorescent A-site RNA, a significant decrease in donor emission at 395 nm and concomitant increase in acceptor emission at 473 nm was observed. However, when unlabeled aminoglycosides were added to the preformed FRET complex, a steady increase in donor fluorescence and concomitant decrease in acceptor emission was observed, indicating competitive displacement of labeled aminoglycosides from the A-site. A three-component FRET system was subsequently assembled using FRET-compatible fluorophores, **7**, coumarin-modified aminoglycoside and Dy547, to determine the relative affinities of aminoglycoside antibiotics to the eukaryotic and prokaryotic decoding sites in a single experiment [140]. Together, these FRET systems facilitate the real-time determination of aminoglycoside binding to A-site, and also provide platforms for screening small-molecule inhibitors by displacement assay.

Internal ribosome entry site (IRES), a highly conserved structural element present at the 5'-UTR of the hepatitis C viral (HCV) RNA genome, binds to the host cell 40S ribosomal subunit and initiates the translation of viral proteins [141]. Guided by crystal structure [142], Hermann and co-workers have replaced a key adenine (A54) residue in the IRES subdomain IIa with 2-AP, and have developed a fluorescence-based assay to monitor the inhibition of HCV replicon by benzimidazole inhibitors (Fig. 4) [143]. Recently, a high-throughput screening protocol using 2-AP fluorescence was established to identify small molecules that bind to the therapeutically important HIV-1 frameshift site RNA [144]. The dynamic central guanosine residue of a conserved GGA bulge present in the frameshift site RNA was

substituted with 2-AP (Fig. 4). Nearly 34 500 small molecules were screened, and 202 compounds, which displayed substantial increase or decrease in 2-AP fluorescence, were identified as initial hits. Subsequent in vitro analysis revealed doxorubicin as one of the tightest binders with low micromolar affinity. Furthermore, this compound was also found to decrease translational frameshifting by ~28 % [144].

Tor and co-workers utilized an emissive uridine analogue based on thieno[3,4-*d*]pyrimidine core (**6**) to monitor the depurination activity of ribosome-inactivating protein (RIP) toxins [50]. RIPs such as ricin and saporin catalyze the depurination of a specific adenosine residue present on a highly conserved ribosomal RNA sequence called α-sarcin/ricin loop (Fig. 4) [145]. The depurination process results in cell death as it lowers the affinity of the ribosome for elongation factors that are necessary for the protein synthesis. The uridine analogue **6**, when placed opposite an abasic site in a model RNA-RNA duplex, positively signaled the presence of an abasic site with remarkable fluorescence enhancement. Drawing inspiration from this observation, several site-specifically labeled emissive RNA constructs that are complementary to various regions of α-sarcin/ricin loop were synthesized. Upon hybridization, one of the modified RNA constructs that is complementary to the entire stem-loop RIPs substrate signaled the depurination activity of the protein [50]. Recently, Hudson and co-workers used a highly fluorescent 6-phenylpyrrolocytidine (**10**) as a molecular beacon-like reporter to monitor the activity of RNase H enzyme [146]. 6-Phenylpyrrolocytidine-incorporated RNA was found to be a very good substrate for HIV-1 reverse transcriptase RNase H enzyme. The rapid cleavage of the RNA substrate was signaled with 14-fold increase in FI.

Micura and co-workers have recently investigated the kinetics of ligand-induced folding of a thiamine pyrophosphate (TPP) responsive bacterial riboswitch (*thiM*) using chemically labeled 2-AP variants [147]. Based on the crystal structure of the ligand-bound aptamer domain [148], seven positions of nucleobases that are vital for the tertiary interactions were chosen for replacement with 2-AP. Corresponding variants of *thiM* RNAs containing site-specific 2-AP labels were generated by enzymatically ligating chemically synthesized short RNA fragments. Changes in 2-AP fluorescence as a function of TPP concentration were used to determine the binding constants of TPP to riboswitch variants [147]. Based on the fluorescence data obtained using labeled variants, a detailed model for the ligand-induced folding process of the *thiM* riboswitch has been proposed. In a similar strategy, Lafontaine and co-worker studied the ligand-induced structural reorganization of *S*-adenosylmethionine (SAM) riboswitch by replacing a key adenine residue with 2-AP in the core region of the aptamer domain [149]. Upon SAM binding, the labeled aptamer undergoes structural reorganization, resulting in strong fluorescence quenching. Using mutant versions of SAM riboswitch and 2-AP fluorescence, the importance of structural elements such as pseudoknot and K-turn on the core domain reorganization has been established.

CONCLUSIONS AND OUTLOOK

It is evident from several publications that there is no lack of creativity when it comes to designing and implementing new fluorescent nucleoside analogues in biophysical assays. The progress has also been accelerated by recent advances in the chemical and enzymatic synthesis of functionalized RNA molecules. Currently, it is possible to assemble RNA molecules with a plethora of modifications almost at any given location. Nevertheless, a few fundamental challenges still exist in implementing an ideal nucleoside probe. Rationally designing a fluorescent nucleoside analogue for a desired application is pragmatically very difficult, because it is "quite" a challenge to predict the photophysical properties of small molecules based on their structures. Moreover, photophysical properties of fluorescent nucleoside analogues can be affected when incorporated into nucleic acids by rigidification–derigidification, solvation–desolvation, and excited-state processes involving neighboring bases. For example, quantum yields of nucleoside probes when incorporated into nucleic acid are most often compromised due to col-

lisional and stacking interactions and or by photoinduced electron-transfer process with neighboring bases.

Ideally, placing the nucleoside reporter near the recognition site, and closely maintaining the native structure and function of the nucleic acid will provide a true picture of the interaction under investigation. In this regard, qualities such as exquisite sensitivity and nonperturbing nature of isomorphic 2-AP riboside have provided excellent fluorescence-based systems to probe the structure, dynamics, and functions of RNA molecules. However, its emission maximum (~370 nm) and low quantum efficiencies when incorporated into nucleic acids greatly limits its applications to in vitro systems only. Therefore, there is a huge demand for the development of nonperturbing nucleoside analogues with improved photophysical properties such as emission in the visible region and high quantum yield when incorporated into nucleic acids. Given the rate at which new RNAs and new functions of RNAs are continuing to be discovered, this demand for new fluorescent ribonucleoside probes with improved photophysical properties will remain strong.

ACKNOWLEDGMENTS

SGS is grateful to the Department of Science and Technology, India, for financial support. AAS is thankful to the Council of Scientific and Industrial Research (CSIR), India, for a graduate research fellowship.

REFERENCES

1. K. Nagai. *Curr. Opin. Struct. Biol.* **6**, 53 (1996).
2. T. Hermann, D. Patel. *Structure* **8**, R47 (2000).
3. S. Jones, D. T. A. Daley, N. M. Luscombe, H. M. Berman, J. M. Thornton. *Nucleic Acids Res.* **29**, 943 (2001).
4. A. Fire, S. Xu, M. K. Montgomery, S. A. Kostas, S. E. Driver, C. C. Mello. *Nature* **391**, 806 (1998).
5. D. Baulcombe. *Nature* **431**, 356 (2004).
6. D. P. Bartel. *Cell* **136**, 215 (2009).
7. R. W. Carthew, E. J. Sontheimer. *Cell* **136**, 642 (2009) and refs. therein.
8. S. Mocellin, R. Costa, D. Nitti. *J. Mol. Med.* **84**, 4 (2006).
9. L. Aagaard, J. J. Rossi. *Adv. Drug Delivery Rev*. **59**, 75 (2007).
10. M. Mandal, R. R. Breaker. *Nat. Rev. Mol. Cell Biol.* **5**, 451 (2004).
11. A. S. Mironov, I. Gusarov, R. Rafikov, L. E. Lopez, K. Shatalin, R. A. Kreneva, D. A. Perumov, E. Nudler. *Cell* **111**, 747 (2002).
12. K. F. Blount, R. R. Breaker. *Nat. Biotechnol.* **24**, 1558 (2006).
13. D. Moazed, H. F. Noller. *Nature* **327**, 389 (1987).
14. U. von Ahsen, J. Davies, R. Schroeder. *Nature* **353**, 368 (1991).
15. T. K. Stage, K. J. Hertel, O. C. Uhlenbeck. *RNA* **1**, 95 (1995).
16. M. L. Zapp, S. Stern, M. R. Green. *Cell* **74**, 969 (1993).
17. S. Wang, P. W. Huber, M. Cui, A. W. Czarnik, H.-Y. Mei. *Biochemistry* **37**, 5549 (1998).
18. M. Daniels, W. Hauswirth. *Science* **171**, 675 (1971).
19. J. M. L. Pecourt, J. Peon, B. Kohler. *J. Am. Chem. Soc.* **122**, 9348 (2000).
20. E. Nir, K. Kleinermanns, L. Grace, M. S. de Vries. *J. Phys. Chem. A* **105**, 5106 (2001).
21. J. Peon, A. H. Zewail. *Chem. Phys. Lett.* **348**, 255 (2001).
22. D. P. Millar. *Curr. Opin. Struct. Biol.* **6**, 322 (1996).
23. M. J. Rist, J. P. Marino. *Curr. Org. Chem.* **6**, 775 (2002).
24. M. E. Hawkins. In *Topics in Fluorescence Spectroscopy, DNA Technology*, **7**, J. R. Lakowicz (Ed.), Kluwer Academic/Plenum Publishers, New York (2003).

25. S. R. Das, R. Fong, J. A. Piccirilli. *Curr. Opin. Chem. Biol*. **9**, 585 (2005).
26. U. Asseline. *Curr. Org. Chem*. **10**, 491 (2006).
27. Y. Tor. *Tetrahedron* **63**, 3425 (2007).
28. R. W. Sinkeldam, N. J. Greco, Y. Tor. *Chem. Rev*. **110**, 2579 (2010).
29. J. N. Wilson, E. T. Kool. *Org. Biomol. Chem.* **4**, 4265 (2006).
30. D. C. Ward, E. Reich, L. Stryer. *J. Biol. Chem.* **244**, 1228 (1969).
31. K. Evans, D. Xu, Y. Kim, T. M. Nordlund. *J. Fluoresc*. **2**, 209 (1992).
32. B. Mennucci, A. Toniolo, J. Tomasi. *J. Phys. Chem. A* **105**, 4749 (2001).
33. A. J. Broo. *Phys. Chem. A* **102**, 526 (1998).
34. J. M. Jean, K. B. Hall. *Proc. Natl. Acad. Sci. USA* **98**, 37 (2001).
35. L. Serrano-Andres, M. Merchan, A. C. Borin. *Proc. Natl. Acad. Sci. USA* **103**, 8691 (2006).
36. E. L. Rachofsky, E. Seibert, J. T. Stivers, R. Osman, J. B. A. Ross. *Biochemistry* **40**, 957 (2001).
37. S. O. Kelley, J. K. Barton. *Science* **283**, 375 (1999).
38. C. Wan, T. Fiebig, O. Schiemann, J. K. Barton, A. H. Zewail. *Proc. Natl. Acad. Sci. USA* **97**, 14052 (2000).
39. S. P. Davis, M. Matsumura, A. Williams, T. M. Nordlund. *J. Fluoresc.* **13**, 249 (2003).
40. M. Kawai, M. J. Lee, K. O. Evans, T. M. Nordlund. *J. Fluoresc.* **11**, 23 (2001).
41. F. Seela, G. Becher. *Helv. Chim. Acta* **83**, 928 (2000).
42. N. J. Greco, Y. Tor. *J. Am. Chem. Soc.* **127**, 10784 (2005).
43. N. J. Greco, Y. Tor. *Tetrahedron* **63**, 3515 (2007).
44. N. J. Greco, Y. Tor. *Nat. Protoc*. **2**, 305 (2007).
45. Y. Tor, S. Del Valle, D. Jaramillo, S. G. Srivatsan, A. Rios, H. Weizman. *Tetrahedron* **63**, 3608 (2007).
46. S. G. Srivatsan, Y. Tor. *J. Am. Chem. Soc.* **129**, 2044 (2007).
47. S. G. Srivatsan, Y. Tor. *Nat. Protoc*. **2**, 1547 (2007).
48. S. G. Srivatsan, Y Tor. *Tetrahedron* **63**, 3601 (2007).
49. S. G. Srivatsan, H. Weizman, Y. Tor. *Org. Biomol. Chem.* **6**, 1334 (2008).
50. S. G. Srivatsan, N. J. Greco, Y. Tor. *Angew. Chem., Int. Ed.* **47**, 6661 (2008).
51. S. G. Srivatsan, Y. Tor. *Chem. Asian J.* **4**, 419 (2009).
52. Y. Xie, A. V. Dix, Y. Tor. *J. Am. Chem. Soc.* **131**, 17605 (2009).
53. Y. Xie, T. Maxson, Y. Tor. *J. Am. Chem. Soc*. **132**, 11896 (2010).
54. D. A. Berry, K.-Y. Jung, D. S. Wise, A. D. Sercel, W. H. Pearson, H. Mackie, J. B. Randolph, R. L. Somers. *Tetrahedron Lett.* **45**, 2457 (2004).
55. R. H. E. Hudson, A. G. Choghamarani. *Nucleosides, Nucleotides Nucleic Acids* **26**, 533 (2007).
56. N. Esho, B. Davies, J. Lee, R. Dembinski. *Chem. Commun.* **4**, 332 (2002).
57. F. Seela. R. Sirivolu. *Org. Biomol. Chem.* **6**, 1674 (2008).
58. M. J. Gait, C. E. Pritchard, G. Slim. In *Oligonucleotides and Analogues: A Practical Approach*, F. Eckstein (Ed.), pp. 25–48, Oxford University Press, Oxford (1991).
59. S. Pitsch, P. A. Weiss, L. Jenny, A. Stutz, X. L Wu. *Helv. Chim. Acta* **84**, 3773 (2001).
60. R. Micura. *Angew. Chem., Int. Ed.* **41**, 2265 (2002).
61. S. A. Scaringe, F. E. Wincott, M. H. Caruthers. *J. Am. Chem. Soc.* **120**, 11820 (1998).
62. S. A. Scaringe. *Methods* **23**, 206 (2001).
63. W. S. Marshall, R. J. Kaiser. *Curr. Opin. Chem. Biol*. **8**, 222 (2004).
64. J. F. Milligan, O. C. Uhlenbeck. *Methods Enzymol.* **180**, 51 (1989).
65. D. M. Jameson, J. F. Eccleston. *Methods Enzymol*. **278**, 363 (1997).
66. S. Verma, F. Eckstein. *Annu. Rev. Biochem.* **67**, 99 (1998).
67. G. Stengel, M. Urban, B. W. Purse, R. D. Kuchta. *Anal. Chem*. **82**, 1082 (2010).
68. J. Ludwig. *Acta Biochim. Biophys. Acad. Sci. Hung.* **16**, 131 (1981).
69. J. A. Piccirilli, T. Krauch, S. E. Moroney, S. A. Benner. *Nature* **343**, 33 (1990).

70. I. Hirao, Y. Harada, M. Kimoto, T. Mitsui, T. Fujiwara, S. A. Yokoyama. *J. Am. Chem. Soc.* **126**, 13298 (2004).
71. R. Rieder, K. Lang, D. Graber, R. Micura. *ChemBioChem* **8**, 896 (2007).
72. C. Höbartner, R. Rieder, C. Kreutz, B. Puffer, K. Lang, A. Polonskaia, A. Serganov, R. Micura. *J. Am. Chem. Soc.* **127**, 12035 (2005).
73. J. R. Williamson. *Nat. Struct. Biol.* **7**, 834 (2000).
74. Y. Yang, M. Kochoyan, P. Burgstaller, E. Westhof, M. Famulok. *Science* **272**, 1343 (1996).
75. K. B. Hall. *Methods Enzymol.* **469**, 269 (2009).
76. J. R. Lakowicz. *Principles of Fluorescence Spectroscopy*, 3rd ed., Springer, New York (2006).
77. B. Valeur. *Molecular Fluorescence, Principles and Applications*, Wiley-VCH, Weinheim (2002).
78. N. J. Turro. *Modern Molecular Photochemistry of Organic Molecules*, University Science Books, New York (2009).
79. K. Börjesson, S. Preus, A. H. El-Sagheer, T. Brown, B. Albinsson, L. M. Wilhelmsson. *J. Am. Chem. Soc.* **131**, 4288 (2009).
80. G. M. Wilson. *Rev. Fluoresc.* 223 (2005).
81. X. Shi, D. Herschlag. *Methods Enzymol.* **469**, 288 (2009).
82. R. A. Tinsley, N. J. Walter. *RNA* **12**, 522 (2006).
83. X. Shi, E. T. Mollova, G. Pljevaljcic, D. Millar, D. Hershlag. *J. Am. Chem. Soc.* **131**, 9571 (2009).
84. C. R. Guest, R. A. Hochstrasser, L. C. Sowers, D. P. Millar. *Biochemistry* **30**, 3271 (1991).
85. T. M. Nordlund, S. Andersson, L. Nilsson, R. Rigler, A. Gräslund, L. W. McLaughlin. *Biochemistry* **28**, 9095 (1989).
86. J. M. Jean, K. B. Hall. *Biochemistry* **41**, 13152 (2002).
87. I. Zagórowska, R. W. Adamiak. *Biochimie* **78**, 123 (1996).
88. M. Menger, T. Tuschl, F. Eckstein, D. Porschke. *Biochemistry* **35**, 14710 (1996).
89. M. Menger, F. Eckstein, D. Porschke. *Nucleic Acids Res.* **28**, 4428 (2000).
90. M. Menger, F. Eckstein, D. Porschke. *Biochemistry* **39**, 4500 (2000).
91. S. R. Kirk, N. W. Luedtke, Y. Tor. *Bioorg. Med. Chem.* **9**, 2295 (2001).
92. N. G. Walter, P. A. Chan, K. J. Hampel, D. P. Millar, J. M. Burke. *Biochemistry* **40**, 2580 (2001).
93. D. A. Harris, D. Rueda, N. G. Walter. *Biochemistry* **41**, 12051 (2002).
94. A. R. Ferre-D'Amare, K. Zhou, J. A. Doudna. *Nature* **395**, 567 (1998).
95. S. Chauhan, R. Behrouzi, P. Rangan, S. A. Woodson. *J. Mol. Biol.* **386**, 1167 (2009).
96. C. Z. Wan, T. B. Xia, H. C. Becker, A. H. Zewail. *Chem. Phys. Lett.* **412**, 158 (2005).
97. L. Zhao, T. Xia. *J. Am. Chem. Soc.* **129**, 4118 (2007).
98. J. D. Ballin, J. P. Prevas, S. Bharill, I. Gryczynski, Z. Gryczynski, G. M. Wilson. *Biochemistry* **47**, 7043 (2008).
99. K. B. Hall, D. J. Williams. *RNA* **10**, 34 (2004).
100. M. J. Rist, J. P. Marino. *Nucleic Acids Res.* **29**, 2401 (2001).
101. J.-I. Tomizawa. *Cell* **38**, 861 (1984).
102. R. Kierzek, Y. Li, D. H. Turner, P. C. Bevilacqua. *J. Am. Chem. Soc.* **115**, 4985 (1993).
103. S. K. Silverman, T. R. Cech. *Biochemistry* **38**, 14224 (1999).
104. M. K. Smalley, S. K. Silverman. *Nucleic Acids Res.* **34**, 152 (2006).
105. A. A. Marti, X. Li, S. Jockusch, Z. Li, B. Raveendra, S. Kalachikov, J. J. Russo, I. Morozova, S. V. Puthanveettil, J. Ju, N. J. Turro. *Nucleic Acids Res.* **34**, 3161 (2006).
106. H. S. Jeong, S. Kang, J. Y. Lee, B. H. Kim. *Org. Biomol. Chem.* **7**, 921 (2009).
107. U. Förster, K. Lommel, D. Sauter, C. Grünewald, J. W. Engels, J. Wachtveitl. *ChemBiochem* **11**, 664 (2010).
108. K. Tanaka, A. Okamoto. *Bioorg. Med. Chem.* **16**, 400 (2008).
109. C.-M. Zhang, C. Liu, T. Christian, H. Gamper, J. Rozenski, D. Pan, J. B. Randolph, E. Wickstrom, B. S. Cooperman, Y.-M. Hou. *RNA* **14**, 2245 (2008).
110. T. Hermann, Y. Tor. *Exper. Opin. Therap. Patents* **15**, 49 (2005).

111. D. Bumcrot, M. Manoharan, V. Koteliansky, D. W. Y. Sah. *Nat. Chem. Biol.* **2**, 711 (2006).
112. S. G. Srivatsan, M. Famulok. *Comb. Chem. High Throughput Screening* **10**, 698 (2007).
113. A. M. Parrott, H. Lago, C. J. Adams, A. E. Ashcroft, N. J. Stonehouse, P. G. Stockley. *Nucleic Acids Res.* **28**, 489 (2000).
114. D. Lazinski, E. Grzadzielska, A. Das. *Cell* **59**, 207 (1989).
115. R. J. Austin, T. Xia, J. Ren, T. T. Takahashi, R. Roberts. *Biochemistry* **42**, 14957 (2003).
116. C. Clerte, K. B. Hall. *Biochemistry* **43**, 13404 (2004).
117. B. Liang, S. Xue, R. M. Terns, M. P. Terns, H. Li. *Nat. Struct. Mol. Biol.* **14**, 1189 (2007).
118. C. Wang, U. T. Meier. *EMBO J.* **23**, 1857 (2004).
119. B. Liang, E. J. Kahen, K. Calvin, J. Zhou, M. Blanco, H. Li. *RNA* **14**, 2086 (2008).
120. M. L. Zapp, M. R. Green. *Nature* **342**, 714 (1989).
121. K. A. Lacourciere, J. T. Stivers, J. P. Marino. *Biochemistry* **39**, 5630 (2000).
122. E. S. DeJong, C. Chang, M. K. Gilson, J. P. Marino. *Biochemistry* **42**, 8035 (2003).
123. T. D. Bradrick, J. P. Marino. *RNA* **10**, 1459 (2004).
124. H. Suryawanshi, H. Sabharwal, S. Maite. *J. Phys. Chem. B* **114**, 11155 (2010).
125. E. Ennifar, J.-C. Paillart, R. Marquet, B. Ehresmann, C. Ehresmann, P. Dumas, P. Walter. *J. Biol. Chem.* **278**, 2723 (2003).
126. D. Muriaux, H. D. Rocquigny, B. P. Roques, J. Paoletti. *J. Biol. Chem.* **271**, 33686 (1996).
127. B. Berkhout, J. L. van Wamel. *J. Virol.* **70**, 6723 (1996).
128. M. J. Rist, J. P. Marino. *Biochemistry* **41**, 14762 (2002).
129. C. Zhao, J. P. Marino. *Tetrahedron* **63**, 3575 (2007).
130. E. Ennifar, J.-C. Paillart, A. Bodlenner, P. Walter, J.-M. Weibel, A.-M. Aubertin, P. Pale, P. Dumas, R. Marquet. *Nucleic Acids Res.* **34**, 2328 (2006).
131. V. K. Tam, D. Kwong, Y. Tor. *J. Am. Chem. Soc.* **129**, 3257 (2007).
132. J. M. Ogle, F. V. Murphy, M. J. Tarry, A. P. Carter, V. Ramakrishnan. *Cell* **111**, 721 (2002).
133. Y. Tor. *Biochimie* **88**, 1045 (2006).
134. S. Shandrick, Q. Zhao, Q. Han, B. K. Ayida, M. Takahashi, G. C. Winters, K. B. Simonsen, D. Vourloumis, T. Hermann. *Angew. Chem., Int. Ed.* **43**, 3177 (2004).
135. M. Kaul, C. M. Barbieri, D. S. Plich. *J. Am. Chem. Soc.* **126**, 3447 (2004).
136. M. Kaul, C. M. Barbieri, D. S. Plich. *J. Am. Chem. Soc.* **128**, 1261 (2006).
137. C. M. Barbieri, M. Kaul, D. S. Plich. *Tetrahedron* **63**, 3567 (2007).
138. J. Parsons, T. Hermann. *Tetrahedron* **63**, 3548 (2007).
139. B. Francois, R. J. M. Russell, J. B. Murray, F. Aboul-ela, B. Masquida, Q. Vicens, E. Westhof. *Nucleic Acids Res.* **33**, 5677 (2005).
140. Y. Xie, A. V. Dix, Y. Tor. *Chem. Commun.* **46**, 5542 (2010).
141. G. A. Otto, J. D. Puglisi. *Cell* **119**, 369 (2004).
142. S. M. Dibrov, H. Johnston-Cox, Y. H. Weng, T. Hermann. *Angew. Chem., Int. Ed.* **46**, 226 (2007).
143. J. Parsons, M. P. Castaldi, S. Dutta, S. M. Dibrov, D. L. Wyles, T. Hermann. *Nat. Chem. Biol.* **5**, 823 (2009).
144. R. J. Marcheschi, K. D. Mouzakis, S. E. Butcher. *ACS Chem. Biol.* **4**, 844 (2009).
145. K. Nielsen, R. S. Boston. *Annu. Rev. Plant Physiol. Plant Mol. Biol.* **52**, 785 (2001).
146. A. S. Wahba, A. Esmaeili, M. J. Damha, R. H. E. Hudson. *Nucleic Acids Res.* **38**, 1048 (2010).
147. K. Lang, R. Rieder, R. Micura. *Nucleic Acids Res*. **35**, 5370 (2007).
148. A. Serganov, A. Polonskaia, A. T. Phan, R. R. Breaker, D. J. Patel. *Nature* **441**, 1167 (2006).
149. B. Heppell, D. A. Lafontaine. *Biochemistry* **47**, 1490 (2008).

